

Extragalactic Cosmic Rays

M. Kachelrieß

Institut for fysikk, NTNU, Trondheim, Norway

I review the status of ultrahigh-energy cosmic ray (UHECR) physics. After introducing the main experimental results and summarizing possible interpretations, I discuss observational and theoretical constraints on the sources of UHECRs. I comment also briefly on the role of magnetic fields. Combining these constraints, I argue that luminous and numerous AGN types as FR-I and Seyfert galaxies, or alternatively hypernovae, are the most promising UHECR sources. Finally, I sketch few of the models presented at the conference before concluding.

*37th International Cosmic Ray Conference -ICRC2021-
15-22 July 2021
Online – Berlin, Germany*

1. Introduction

A review with the title “Extragalactic Cosmic Rays” requires first to clarify the lowest energies to be included, what in turn depends on the question where the transition between Galactic and extragalactic CRs takes place. I will later argue that this transition happens around 5×10^{17} eV. To be definite, I call ultra-high energy cosmic rays (UHECR) all particles with energies above 10^{17} eV. I start with a discussion of the basic experimental results in Sec. 2, before I comment briefly on the role of magnetic fields in Sec. 3. Then observational and theoretical constraints on the sources of UHECRs are discussed in Sec. 4. Finally, I sketch a small selection of the UHECR models presented at this ICRC.

2. Observations and their interpretation

2.1 Energy spectrum

In Fig. 1, measurements of the UHECR intensity $I(E)$ from the two experiments with the largest exposure, the Pierre Auger Observatory (PAO) and the Telescope Array (TA) are presented [1]. The uncertainty in the absolute energy scale of these experiments is around 10%, leading to large shifts in a plot of $E^3 I(E)$. The two experiments can be cross-calibrated using the fact that the UHECR intensity up to 10^{19} eV is very isotropic: Applying a relative shift of the energy scale of the two experiments, their all-particle intensities shown in the left panel of Fig. 1 averaged over their full field of view agree well up to 3×10^{19} eV. At higher energies, the deviations increase, with the cutoff in the TA spectrum shifted to higher energies. The agreement at the highest energies improves in the declination band common to the two experiments shown in the right panel, but some differences persists. Their elimination would require an energy-dependent rescaling. In addition, TA sees slightly different spectra in the southern and northern part of its sky. Apart from unaccounted systematic effects, the imprint of the large-scale structure (LSS) on the source distribution which is not averaged out at these energies could explain this difference. Moreover, variations in the maximal energies of the most important sources in different parts of the sky can

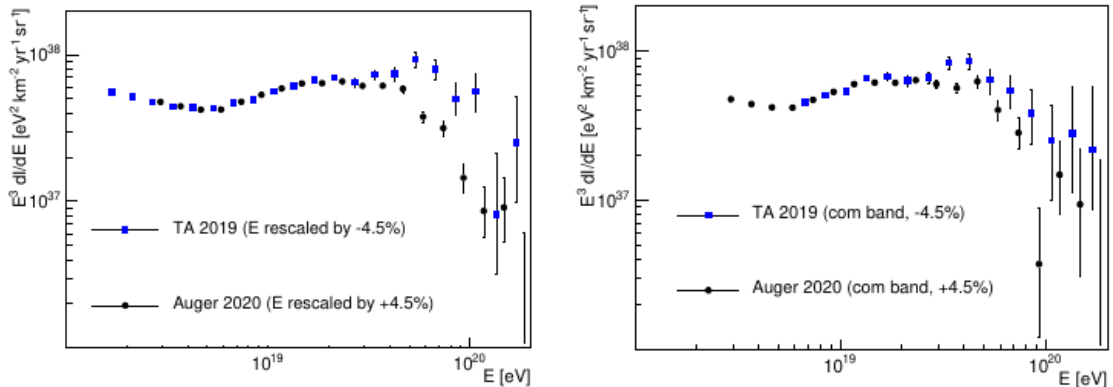


Figure 1: UHECR spectrum measured by the PAO (Auger) and TA experiments after a constant relative shift by 9.0%; Left panel full field of view and right panel in the common declination band; from Ref. [1].

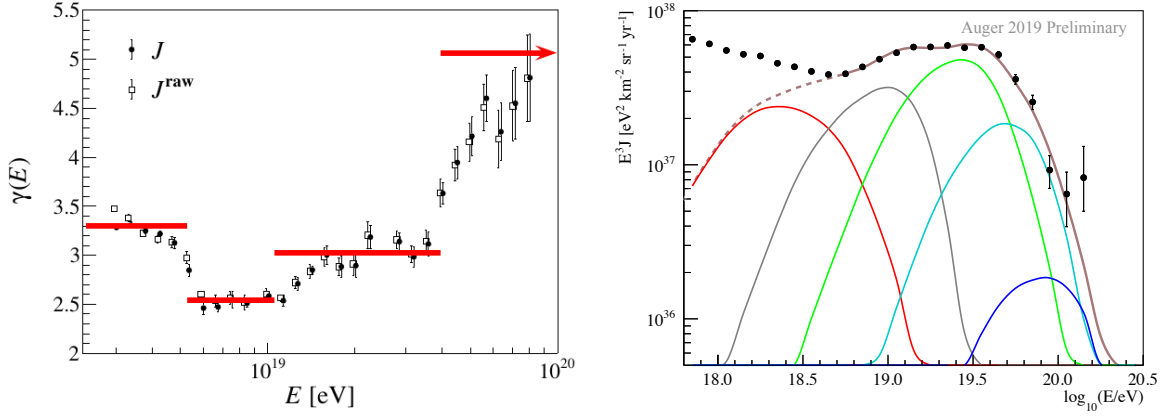


Figure 2: Left: Local fit of power-law index to the CR intensity measured by the PAO compared to the index obtained using “four segments” (red line). Right: A model fit to both spectrum and composition data [5].

become important. Alternatively, when the cutoff is caused by the GZK effect, differences in the distance to the dominating sources may cause an intensity difference. Note that the energy $E_{1/2} \simeq 5 \times 10^{19}$ eV where the integral intensity drops for a pure proton composition by a factor two relative to the intensity expected without pion production [2] deviates significantly from the value determined from the PAO data, $E_{1/2} \simeq (2.3 \pm 0.4) \times 10^{19}$ eV. Such a low value of $E_{1/2}$ points to an intermediate mass composition at the highest energies, if the suppression is a propagation effect.

The energy spectrum of CRs above 10^{17} eV shows several features. The second knee around $E \simeq 5 \times 10^{17}$ eV, the ankle at $E \simeq 3 \times 10^{18}$ eV and a flux suppression at the highest energies. An additional feature, the so-called instep, has been recently established by the PAO [3, 4]. In the left panel of Fig. 2, the slopes obtained fitting a power-law with four segments to the data are compared to the varying slope derived by fitting the spectrum locally including three to six energy bins. This comparison shows clearly that, given the small experimental errors, broken power laws are not an adequate description of the energy spectrum.

2.2 Composition

The mass composition of UHECRs can be inferred from the atmospheric depth X_{\max} where the number of particles in an air shower reaches its maximum. In the left panel of Fig. 3, the X_{\max} values obtained by the PAO using fluorescence detectors (FD) are presented¹ as filled dots. Additionally, results from the surface array (SD) are shown as open dots. From the evolution of X_{\max} with energy, one can conclude that the composition becomes lighter between $10^{17.2}$ and $10^{18.33}$ eV, qualitatively in agreement with the expectation for a transition from Galactic to extragalactic CRs in this energy region. Above $10^{18.33}$ eV, this trend is reversed and the composition becomes heavier. The X_{\max} data from TA shown by squares are approximately corrected for detector effects by shifting the mean by $+5 \text{ g/cm}^2$ [11], as well as shifted down by 10.4% in energy. After accounting for these corrections, the X_{\max} data from the two experiments are in good agreement. In the right panel of Fig. 3, the width $\sigma(X_{\max})$ of the X_{\max} distributions is shown. Again, the $\sigma(X_{\max})$ distribution from TA has to be corrected for the detector resolution. A wide distribution as obtained at low energies

¹Unfortunately, no update of the common PAO and TA working group on composition was presented at his ICRC.

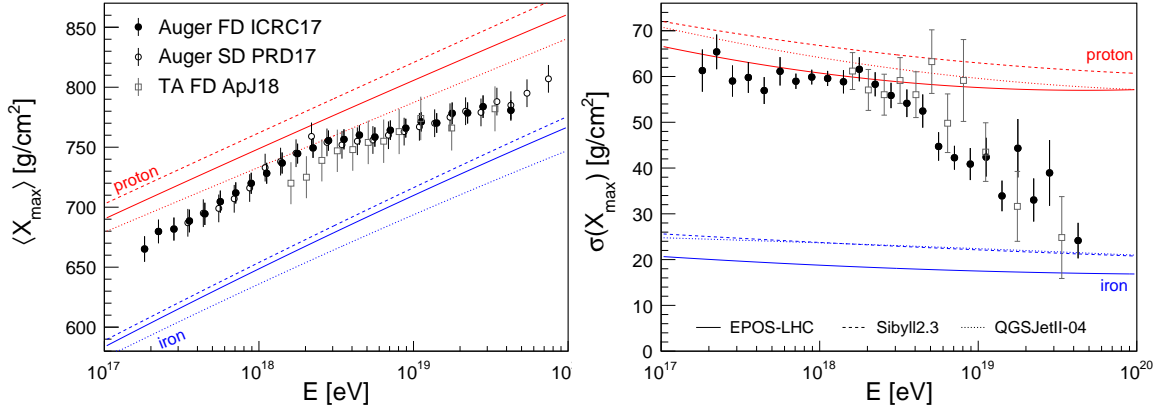


Figure 3: Measurements [6–8] of the mean (*left*) and standard deviation (*right panel*) of the distribution of shower maximum as a function of energy. The energy evolution of the mean and standard deviation of X_{\max} obtained from simulations [9] are shown as red and blue lines; from Ref. [10].

can be caused either by a light or a mixed composition. At higher energies, the distribution becomes more narrow, pointing to a purer and heavier composition.

Using simulations for hadronic interactions, one can compare the predicted X_{\max} distributions for a mixture of CR nuclei to the observed distribution and fit the relative fraction of the CR nuclei. The result of such a fit for a mixture of proton, helium, nitrogen and iron nuclei is shown in Fig. 4. Above 10^{18} eV, the dominant component in the UHECR flux changes successively from protons, to helium and nitrogen, a behaviour suggestive for the presence of a Peters cycle. At the lowest energies, there is evidence for a non-zero iron fraction which drops then to zero.

A fit of the combined PAO data on the energy spectrum and the composition has been presented in Ref. [3]. In this fit, the extension of the third segment corresponds to the one expected from the charge ratio between CNO and He. In order to obtain a clean separation of the mass groups, a very hard slope² of the injection spectrum into extragalactic space is required: For instance, the fits presented in Ref. [14] use slopes for $dN/dE \propto E^{-\alpha}$ with α between $\simeq -1$ and -2 . Moreover, the ankle has to be explained by a second extragalactic population which does not show the same Peters cycle but has a dominantly light composition. An alternative explanation for the instep is that it is just the most obvious of several irregularities which are caused by the small number of sources contributing to the high-energy end of the energy spectrum.

2.3 Anisotropies and correlations

Expectations A priori, four sub-classes of possible anisotropies were expected to be imprinted on the arrival directions of extragalactic cosmic rays (see e.g. Ref. [16]): i) At energies high enough such that deflections in magnetic fields are sufficiently small, UHECR sources may reveal themselves as small-scale clusters of UHECR arrival directions. This requires a low density of UHECR sources so that the probability to observe several events of at least a subset of especially bright sources is large enough. ii) At lower energies, the energy-loss horizon of UHECRs and thereby the number of sources visible increases. At the same time, deflections in magnetic fields

²Steep escape spectra may be generated by threshold effects of $A\gamma$ interactions in the source, see, e.g., [12, 13].

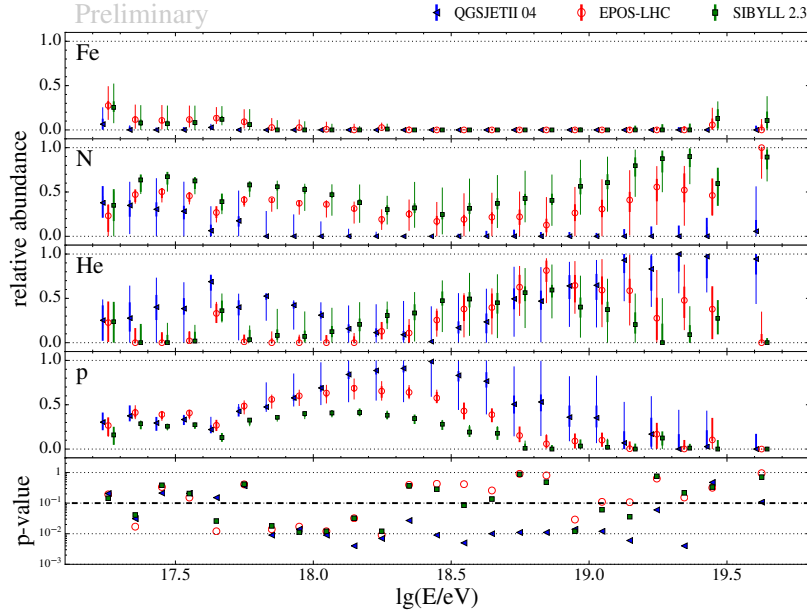


Figure 4: Fraction of the four elements in the UHECR flux; from Ref. [15].

become more important. While thus individual sources cannot be identified anymore, anisotropies on medium scales should reflect the inhomogeneous distribution of UHECR sources which in turn is connected—although in a biased way—to the observed LSS of matter. iii) At even lower energies, also anisotropies on medium scales disappears, both because the inhomogeneities in the source distribution will be averaged out because of the increased energy-loss horizon of UHECRs and because of deflections. Thus the CR sky appears isotropic, except for a dipole anisotropy of 0.6% induced by the cosmological Compton-Getting (CCG) effect [17]. iv) Finally, the Galactic magnetic field (GMF) can induce anisotropies in the observed flux of extragalactic UHECRs (even if it is isotropic at the boundary of the Milky Way), for rigidities low enough that regions disconnected from spatial infinity in the CR phase space exist. According to the estimate of Ref. [18] anisotropies of this kind should be expected in models that invoke a dominating extragalactic component already at $E/Z \simeq 4 \times 10^{17}$ V, if the GMF contains a dipole component.

Obviously, it is not guaranteed that all these four anisotropies can be observed. If the average charge of UHECR primaries, their source density and/or extragalactic magnetic fields (EGMF) are too large, the integrated flux above the energy where point sources become visible may be too small for the present generation of UHECR experiments. Similarly, the presence of a magnetic horizon may replace the CCG effect by one due to the peculiar flows of nearby galaxies. It was conjectured that the experimentally easiest accessible anisotropies are the medium-scale anisotropies connected to the LSS of UHECR sources [19, 20]. However, at present, the only detected anisotropy with more than 5σ is the dipole moment which is the anisotropy most robust against deflections. Clearly, the impact of magnetic fields is more important than expected, partly because the composition is not proton-like as assumed earlier.

Dipole anisotropy The dipole anisotropy δ (projected into the equatorial plane) and its phase have been measured starting from TeV energies. Below 10^{17} eV, the phase of the anisotropy is

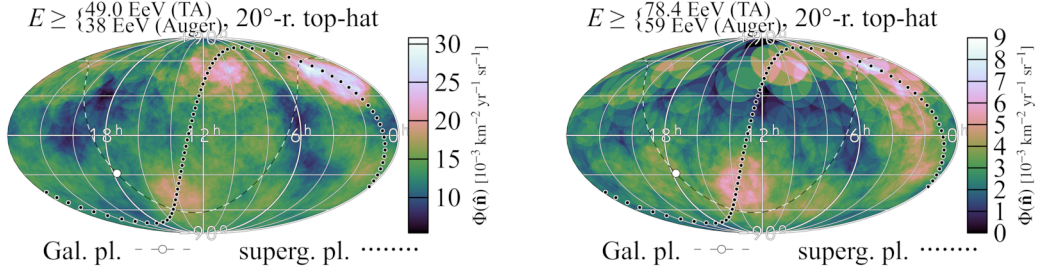


Figure 5: The UHECR intensity in equatorial coordinates averaged over 20° , left above $E = 38$ EeV using the PAO energy scale, right above 59 EeV, from Ref. [25].

approximately constant, except for a flip at ≈ 200 TeV. By contrast, at energies above 10^{17} eV, the phase changes smoothly towards 100 degrees in right ascension (R.A.), i.e. it points roughly towards the Galactic anticentre. This suggests that the extragalactic CR flux starts at 10^{17} eV to become sizable. The strength of the dipole at higher energies could be measured only in 2017 for the first time by the PAO: Performing a one-dimensional harmonic analysis in R.A. and splitting the events in two energy bins, 4–8 EeV and > 8 EeV [21, 22], the amplitude $6.5^{+1.3}_{-0.9}\%$ in the second energy > 8 EeV deviates by more than 5σ from isotropy. Thus the observed amplitude of the dipole anisotropy is a factor ten larger than the one expected for the CCG effect. The estimated direction may be connected to an overdensity in the local galaxy distribution, seen e.g. in the 2MRS catalogue [23]. Higher-order harmonics like the quadrupole moment are consistent with isotropy. Combining data from PAO and TA allows one to derive the multipole moments without imposing additional hypotheses [24]: The results are compatible with those using only PAO data, but with uncertainties about twice as small for the z components of the dipole and quadrupole moment.

Medium scale anisotropies In Fig. 5, we show a sky map combining events above two selected energy thresholds, averaged over 20° -radius top-hat windows, from the TA and PAO experiments [25]. While the significance feature of the the “TA hotspot”, which is centered at R.A. $\approx 150^\circ$ and dec $\approx 40^\circ$, has diminished relative to the ICRC-2017, the two additional “warm spots” in the field-of-view of the PAO have become more prominent. One of them coincides with Cen A and both overlap with the supergalactic plane.

Correlations An alternative method to search for UHECR sources are correlation studies. The recent analysis [26] of the PAO data showed evidence for a correlation of the arrival directions of UHECRs with starburst galaxies, i.e. galaxies which are characterized by exceptionally high rates of star formation. Specifically, for UHECR with observed energies $E > 39$ EeV, a model which attributes 9.7% of the UHECR flux to nearby starburst galaxies (and the remaining 90.3% to an isotropic background) was found to be favoured, with 4σ significance, over the isotropic hypothesis. About 90% of the anisotropic flux was found to be associated to four nearby starburst galaxies: NGC 4945, NGC 253, M83, and NGC 1068. Alternatively, a correlation analysis with 17 bright nearby AGNs was performed. Here, the warm spot is related to Cen A and around 7% of the total flux is attributed to the selected AGNs. At this conference, the PA and the TA collaborations presented a combined search for this signal [27]. The correlation between the arrival directions of $12^{+5}_{-3}\%$ of cosmic rays detected with $E \geq 38$ EeV by Auger and with $E \geq 49$ EeV by TA and

the position of nearby starburst galaxies has a 4.2σ post-trial significance, when the directions are smeared over $15.5^{+5.3}_{-3.2}^\circ$ angular scales. Thus this combined analysis has a stronger significance than the Auger-only data but is still short of the discovery level. In addition, a weaker correlation with the overall galaxy distribution, or equivalently with the supergalactic plane, was found.

Note that some starburst galaxies, such as NGC 1068 and NGC 4945, show a dominant non-thermal contribution from their central regions, indicating an active black hole. The presence of such AGN-starburst composites may affect in turn the interpretation of correlation analyses like the one of Ref. [26]. Moreover, the formal significance of correlation studies has to be taken with a grain of salt, as the look-elsewhere effect due to unpublished unsuccessful searches is impossible to quantify. New data from TA_x4 and AugerPrime will be therefore important to test these correlations.

2.4 Transition energy

The question at which energy the transition from Galactic to extragalactic CRs takes place is essential for the understanding of the requirements on the acceleration mechanisms of Galactic CR sources as well as for the determination of the nuclear composition and the injection spectrum of extragalactic sources. In the past, the transition energy has been usually associated with one of the two evident features of the UHECR spectrum: The second knee around $E \simeq (1 - 5) \times 10^{17}$ eV or the ankle at $E \simeq 3 \times 10^{18}$ eV. The latter choice offered a simple explanation for the sharpness of the ankle as the cross-over between the end of Galactic flux and the start of the extragalactic component. It allowed also for an extragalactic injection spectrum $Q(E) \propto 1/E^\beta$ with $\beta \approx 2$, i.e. close to the expectation for diffusive shock acceleration. However, this suggestion clearly challenges acceleration models for Galactic CR sources. Moreover, this solution leads to the following ‘‘coincidence problem’’: Since the acceleration and diffusion of CRs depends only on rigidity, the end of the Galactic CR spectrum consists of a sequence of cutoffs at ZE_{\max} , i.e. it follows a Peters cycle. If the knee in the total CR spectrum marks the suppression of Galactic CR protons, then the second knee should correspond to the iron knee. Thus, in this interpretation, the second knee signals the end of the Galactic iron flux from those sources which contribute the bulk of Galactic CRs. Therefore an additional Galactic population of CR sources would be required to fill the gap between the second knee and the ankle. If this population is unrelated to the standard population of Galactic CR sources, it is surprising that the normalisation and the slope of the two fluxes is so similar.

Models identifying the second knee as the transition to extragalactic CRs have to postulate two different extragalactic source populations, implying again the ‘‘coincidence problem’’ described above. This problem may be avoided if a source type consists of two sub-populations. Alternatively, these models have to implement a physical mechanism which explains the ankle as a consequence of either the propagation of extragalactic CRs or of interactions in their sources. The first successful model of this kind, the dip model [28], requires an almost pure ($\gtrsim 90\%$) proton flux and is therefore excluded by composition measurements. Viable alternative models which rely on interactions of CR nuclei inside CR sources have been proposed [12, 13].

How can these two options for the transition energy, the second knee and the ankle, be experimentally distinguished? It is natural to expect that the nuclear composition of Galactic and extragalactic CRs should differ, because of propagation effects and of the different nature of their sources. In particular, the Galactic CR spectrum should become close to its end iron-dominated.

A similar behaviour is expected for the extragalactic flux, shifted however to higher energies. Thus one expects the extragalactic composition at the transition energy to be lighter than the Galactic one. Therefore the signature of the transition in the composition is the disappearance of the (Galactic) iron, and the increase of a light or intermediate extragalactic component. Using only the composition data, the limits on the iron fraction from Fig. 4 imply that the Galactic contribution to the observed CR spectrum has to die out before 7×10^{17} eV. Combining composition and anisotropy measurements strengthens this conclusion considerably: In Ref. [29], it was shown that a light (intermediate) Galactic CR flux leads to a dipole of order 20% (10%), overshooting clearly the limits which are on the percent level [22]. Thus the dominant light-intermediate contribution to the CR flux measured by the PAO above 3×10^{17} eV has to be extragalactic. Finally, we recall that the smooth change of the dipole phase at energies above 10^{17} eV towards the Galactic anticentre supports the suggestion that the transition from Galactic to extragalactic CRs starts at 10^{17} eV. Thus we conclude that the second knee marks the transition between Galactic and extragalactic CRs. Then it is natural that the second knee is close to its upper end of the range $(1 - 5) \times 10^{17}$ eV of values considered in the literature, what agrees with the value $E \simeq (5.0 \pm 0.8) \times 10^{17}$ eV determined in Ref. [4].

2.5 Secondary photon and neutrino fluxes

High-energy cosmic rays can interact with gas or photons in their sources, and with photons from the extragalactic background light (EBL) during propagation. The production of neutrinos is by isospin symmetry tied to the one of photons, and both depend in turn on the flux of primary CRs. Therefore the observation of these CR secondaries can provide important information on extragalactic CRs.

Cosmogenic neutrinos are mostly produced in interactions on EBL photons with energy $\varepsilon_\gamma \lesssim 10$ eV. With $\langle E_\nu \rangle = E_p/20$, the energy threshold of this reaction implies that the flux of cosmogenic neutrinos is suppressed below $E \approx 2 \times 10^{17}$ eV. If neutrinos are produced by $p\gamma$ interactions in the source, e.g. on radiation from an accretion disk with $\varepsilon_\gamma \lesssim 1$ eV, one expects as threshold $E_{\text{th}} \approx 2 \times 10^{18}$ eV. In contrast, pp interactions lead to a neutrino flux without threshold. While neutrinos reach the observer unabsorbed, gamma-rays with energies in the TeV region and above initiate electromagnetic cascades, via the processes $\gamma + \gamma_b \rightarrow e^+ + e^-$ and $e^\pm + \gamma_b \rightarrow e^\pm + \gamma$ [30, 31]. This cascade develops very fast until it reaches the pair creation threshold. Thus the Universe acts as a calorimeter for electromagnetic radiation, accumulating it in the MeV-TeV range as an extragalactic gamma-ray background (EGRB). Measurements of the EGRB by Fermi-LAT [32] were used to constrain strongly evolving UHECR models [33–35]. In particular, the limit on the allowed energy density of the cascade radiation, $\omega_{\text{casc}} \leq 2 \times 10^{-7}$ eV/cm³, bounds the extragalactic neutrino flux [34].

In Ref. [37], the Fermi collaboration concluded that up to 86% of the EGRB is emitted by unresolved blazars. Taking this result at face value, the room for any additional injection of photons is very limited. It is therefore desirable that the same source class explains both UHECRs and the observed neutrino flux by IceCube. In Fig. 6, the expectations from Ref. [36] for the secondary photon and neutrino fluxes produced by UHECR sources are shown. The EGRB measurements (blue errorbars) limit the secondary photon flux from UHECR sources which has a universal shape indicated by the orange band [38, 39]. The total UHECR flux is shown by violet error-bars, while

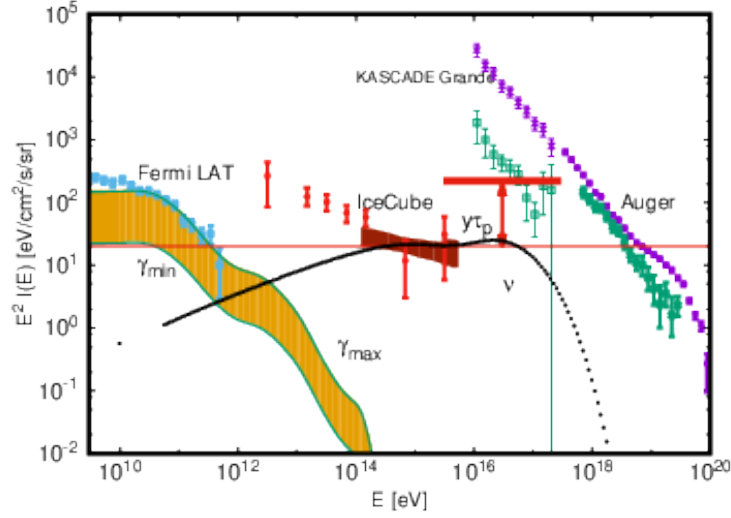


Figure 6: Expected secondary photon and neutrino fluxes from UHECR sources compared to the EGRB measured by Fermi-LAT, diffuse neutrino flux by IceCube and the all-particle and proton fluxes by KASCADE Grande and PAO. The neutrino flux example shown as thin dotted line is from Ref. [13]; adapted from Ref. [36].

the green error-bars give the flux of UHECR protons derived from the PAO and KASCADE-Grande composition measurements [15, 40]. The red points and band represent neutrino measurements by IceCube [41, 42]. The horizontal thin red line shows the average neutrino flux level in the case of an $1/E^2$ flux, which is of the order of 10% of the EGRB. In the case of an $1/E^{2.15}$ neutrino flux, the accompanying photons saturate the gamma-ray bound. The thick red line shows the expected level of the proton flux required to produce the diffuse neutrino flux. The ratio $y\tau_p$ of the proton and neutrino fluxes is determined by the corresponding proton interaction probability τ_p and the spectrally weighted average energy transfer $\langle y \rangle$ to neutrinos. For a spectral slope close to two, $y \approx 0.2$, implying that a large fraction of protons has to interact inside their sources. While the high-energy part of the astrophysical neutrino flux is consistent with $\alpha \approx 2.1$ and a normalisation close to the cascade bound, at lower energies a softer component appears. The sources of this soft component have to be either extragalactic and hidden, or Galactic but close to isotropically distributed. Extensive discussions of this connection between extragalactic cosmic ray sources and the observed high-energy neutrino flux can be found in the contributions of the Multi-Messenger track at this conference [43].

3. Remarks on the role of magnetic fields

The strength of the Galactic and extragalactic magnetic fields plays a crucial role for the identification of UHECR sources: In addition to the obvious effect of deflections, the resulting time-delays determine the effective source density of transient sources. Moreover, these delays may undermine the selection of potential UHECR sources based on properties of their electromagnetic spectrum, if the delays become larger than the activity periods of the sources.

Galactic magnetic field Tess Jaffe discussed extensively our knowledge about the GMF in her review talk [44]. It is therefore sufficient to note here that the various GMF models differ by putting emphasis on rotation measures of extragalactic sources or of Galactic pulsars. The former models should therefore provide generally a better description of the magnetic field in the Galactic halo, while the latter should perform better in the Galactic plane. However, for none of these GMF models, the coherence length and the (relative) strength of the regular and the turbulent field are constrained such that the escape time of Galactic cosmic rays reproduces the measured secondary-to-primary ratios below the knee. Consequently, these models cannot be used to investigate, e.g., the transition between Galactic and extragalactic cosmic rays or the knee without adjusting these parameters [45].

Extragalactic magnetic field The origin of the EGMF is one of the outstanding questions in astrophysics. Its seed fields may be generated in the primordial universe or by astrophysical processes like galactic plasma outflows. If the field strength of the EGMF is normalised in both cases such to reproduce observations in the cores of galaxy cluster, their filling factors differ drastically. Observationally, the strength of the EGMF is limited independent of its creation mechanism by 2×10^{-9} G from rotation measures [46], while the present strength of fields with a primordial origin is restricted to 5×10^{-11} G from CMB anisotropies [47]. The existence of hot spots in the UHECR flux, if they can be firmly established, provides an alternative way to derive upper limits on the EGMF. There exists also lower limits on the strength and the filling factor of the EGMF [48]. However, it has been argued that they are invalidated by plasma instabilities [49].

If the average deflection angle per correlation length L_c is small, $R_L \gg L_c$, the CR propagation resembles a random walk in the small-angle regime and the variance of the deflection angle after the distance d is given by

$$\vartheta_{\text{rms}} \equiv \langle \vartheta^2 \rangle^{1/2} \simeq \frac{(2dL_c/9)^{1/2}}{R_L} = 25^\circ Z \left(\frac{10^{19} \text{eV}}{E} \right) \left(\frac{d}{100 \text{Mpc}} \right)^{1/2} \left(\frac{L_c}{1 \text{Mpc}} \right)^{1/2} \left(\frac{B}{10^{-9} \text{G}} \right). \quad (1)$$

The increased path-length compared to straight-line propagation leads to the time-delay

$$\Delta t \simeq \frac{d\vartheta_{\text{rms}}^2}{4} = 1.5 \times 10^3 \text{yr} Z^2 \left(\frac{10^{20} \text{eV}}{E} \right)^2 \left(\frac{d}{10 \text{Mpc}} \right) \left(\frac{L_c}{1 \text{Mpc}} \right) \left(\frac{B}{10^{-9} \text{G}} \right)^2 \quad (2)$$

of charged CRs relative to photons [50, 51]. This increase can result in the formation of a magnetic horizon [52, 53]: The maximal distance a CR can travel is in the diffusion picture given by $r_{\text{hor}}^2 = \int_0^{t_0} dt D(E(t))$ where t_0 is the source age. If we assume that a magnetic field with correlation length $L_c \sim \text{Mpc}$ and strength $B \sim 0.1 \text{nG}$ exists in a significant fraction of the Universe, then the size of the magnetic horizon at $E = 10^{18} \text{eV}$ is $r_{\text{hor}} \sim 100 \text{Mpc}$. Hence, similar to the GZK effect at high energies, we see a smaller and smaller fraction of the Universe for lower CR energies. As a consequence, the spectrum of extragalactic CRs visible to us hardens and the extragalactic component becomes suppressed.

4. Sources, general constraints and their modelling

4.1 Observational constraints

The observed UHECR intensity fixes the required emissivity \mathcal{L} of the UHECR sources, i.e. their energy input per volume and time, up to a model-dependent factor of order one. For the fit presented in Fig. 2, the PAO determined the emissivity above the ankle, $E > 5 \times 10^{18}$ eV, at the present epoch as $\mathcal{L} \simeq 6 \times 10^{44}$ erg/(Mpc³ yr). If the transition to extragalactic CRs is early, as we argued above, the corresponding emissivity increases by at least one order of magnitude. For concreteness, we will use $\mathcal{L} = 1 \times 10^{46}$ erg/(Mpc³ yr) for the following estimates. In the case of a unique source class, the relation $\mathcal{L} = Ln_s$ implies that in a plot of luminosity L vs. number density n_s potential source classes have to sit along a fixed diagonal. If several source classes contribute significantly to the total emissivity, they can lie below this diagonal.

The absence of small-scale clustering in the UHECR arrival directions implies that the source density—or deflections in magnetic fields—are sufficiently large. Performing an autocorrelation analysis of the PAO events with $E > 70$ EeV, the bounds $n_s > 5 \times 10^{-4}$ /Mpc³ for a separation angle $\vartheta = 3^\circ$ and $n_s > 6 \times 10^{-6}$ /Mpc³ for $\vartheta = 30^\circ$ were derived³ in Ref. [54]. At these energies, sources should be within 200 Mpc and one does not expect from Eq. (1) deflections larger than 20° even for the strongest allowed field. Thus we will use the limit $n_s > 3 \times 10^{-5}$ /Mpc³ for the density of UHECR sources. For comparison, the density of the X-ray selected powerful AGNs with X-ray luminosity $L > 10^{43}$ erg/s in the energy range (0.2–5) keV equals $n_s \sim (1–5) \times 10^{-5}$ /Mpc³ within redshift $z \lesssim 0.02$, while the number of Seyfert galaxies is a factor 20 higher [55]. Normal galaxies have a density of $n_s \sim 10^{-2}$ /Mpc³.

4.2 Constraints from theory

Potential sources of UHECRs have to satisfy as two general constraints the Hillas and Blandford conditions. Combined with measurements of the present energy density of UHECRs and the absence of small-scale anisotropies, the Blandford criterium leads to stringent constraints on the number density of these sources.

Hillas condition The Larmor radius $R_L = E/(ZeB)$ of accelerated particles has to fit inside the accelerator of size R_s which confines the particles by a magnetic field with strength B , i.e. $R_L = E/(ZeB) \leq R_s$. For known magnetic fields and source sizes, one can constrain thus the maximal achievable energy as $E_{\max} = \Gamma ZeBR_s$, a constraint shown in the Hillas plot of Fig. 7 for a compilation of potential cosmic ray sources. The Lorentz factor $\Gamma = (1 - \beta^2)^{1/2}$ introduced in E_{\max} accounts for a possible relativistic bulk motion of the source and is probably only for gamma-ray bursts and blazars a significant correction. Sources able to accelerate protons to $E > 10^{20}$ eV should lie above the solid red line, while sources above the green line can accelerate iron up to 10^{20} eV. Clearly, a heavy composition of UHECRs alleviates considerably the acceleration problem of UHECRs. The main uncertainty in this plot is the strength of the source magnetic field, since nonlinear processes typically lead to an amplification of magnetic fields inside the source. This effect is taken partly into account in Fig. 7, but its exact magnitude is uncertain. Synchrotron energy

³As these limits constitute strong constraints on possible UHECR sources, an update and a more detailed study of the impact of the EGMF are highly desirable.

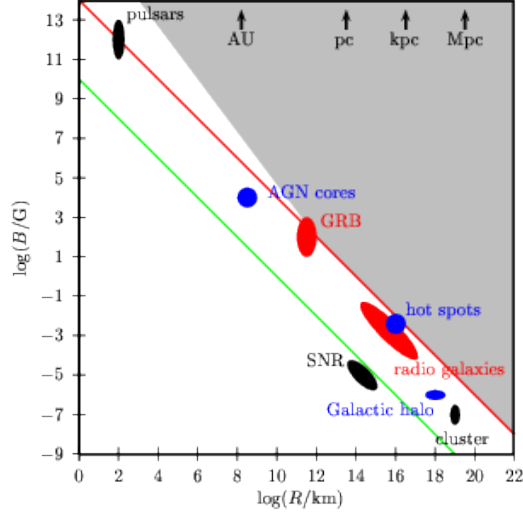


Figure 7: Magnetic field strength B versus size R of various CR sources; adapted from Refs. [56, 57].

losses reduce the allowed area for protons to the grey area. In addition, the finite acceleration time disfavours large sources. Thus in general, sources neither too small (minimizing energy losses) nor too big (avoiding too long acceleration times) are favored.

Blandford condition Constraints on the minimal luminosity of a source able to accelerate CRs up to a certain energy have been derived for specific source types and acceleration mechanisms [58–61], starting from the work of Lovelace [58] on radio galaxies. Blandford stressed first the universality of these limits in Ref. [59], and we will call this bound on the luminosity of a cosmic ray source therefore the Blandford condition.

Let us illustrate this requirement using the simplest example, the acceleration of charged particles by a regular electric field: The acceleration of protons to the energy $E = 10^{20}$ eV requires the potential difference $U = 10^{20}$ V. What is the minimal power P dissipated by such an accelerator? In order to use the basic equation $P = UI = U^2/R$ learnt in high-school, we have to know the appropriate value of the resistance R . Since an accelerator operates at densities close to vacuum, we use $R \sim 1000 \Omega$ (guided by the “impedance of the vacuum”, $R_0 = 4\pi k_0/c = 1/(\epsilon_0 c) \simeq 377 \Omega$). Hence a source able to produce protons with $E = 10^{20}$ eV by acceleration in a regular electromagnetic field has the minimal luminosity $L = U^2/R \gtrsim 10^{37}$ W = 10^{44} erg/s. Including the effect of possible bulk motions and relaxing the maximal energy, the bound becomes

$$L \gtrsim 3 \times 10^{42} \text{ erg/s} \frac{\Gamma^2}{\beta} \left(\frac{E/Z}{5 \times 10^{18} \text{ eV}} \right)^2. \quad (3)$$

How does this derivation apply, e.g., to diffusive shock acceleration? This case corresponds to a “circular accelerator”, with an energy gain at each crossing of the shock front. Microscopically, the electric field in the fluid frame which is generated by the plasma flow in the shock region accelerates charged particles at each crossing of the shock region. Thus the same argument as above applies.

Note also that $R_0 = c\mu_0$ transforms $P = U^2/R_0$ into an equivalent (assuming the limit $\beta \sim 1$), often used form involving the magnetic energy density.

The bound (3) on L can be used to obtain an upper limit on the density n_s of UHECR sources, since the observed UHECR intensity fixes the required emissivity $\mathcal{L} = n_s L$. Hence, the density of stationary UHECR sources able to accelerate protons to $E = 5 \times 10^{18}$ eV should be smaller than $n_s < \mathcal{L}/L \simeq 1 \times 10^{-4}/\text{Mpc}^3 \Gamma^{-2}$.

4.3 Combined constraints on the luminosity and number density of UHECR sources

Stationary sources We combine now in the left panel of Fig. 8 for stationary sources the lower bound on n_s to avoid small-scale clustering, $n_s > 3 \times 10^{-5}/\text{Mpc}^3$ (for the case of strong EGMFs), the lower bound on the luminosity and the requirement to reproduce the observed emissivity. The first condition excludes the grey area on the left, while the second requirement excludes (assuming $\Gamma = 1$) additionally the yellow area at the bottom. Only one source class, FR-I radio galaxies, satisfy both constraints: Taking into account in addition their non-zero bulk Lorentz factors, their luminosity is above the Blandford limit.

How could these conditions be relaxed to allow for more potential UHECR sources? If a second source populations is responsible for the the extragalactic CR flux below the ankle, then the requirement on the emissivity of the first UHECR population is reduced by a factor 20. In addition, the total energy dissipated in electromagnetic radiation is larger than in the X -ray band used as our proxy, $L_{\text{em}} = L_X + \dots$. Adapting these changes promotes also Seyfert galaxies or low-luminosity AGNe to possible UHECR sources.

Bursting sources The effective number density of bursting sources with rate R and observed burst duration τ is given by $n_s \simeq 3R\tau/5$ [62]. The burst duration τ is dominated by the time delays in magnetic fields: Using $E = 70 \text{ EeV}$, i.e. the lower energy used to bound n_s from small-scale clustering, together with $B = 10^{-11} \text{ G}$ gives $\tau \simeq 6 \times 10^4 \text{ yr}$ and $R = 5n_s/(3\tau) \gtrsim 3 \times 10^{-9}/\text{Mpc}^3/\text{yr}$. The luminosity bound is for bursting sources as GRBs not a severe restriction, since the true burst time is much smaller than the observed duration τ . However, since these sources are rare, they can typically not provide the observed UHECR emissivity, i.e. they are below the line $L_{\text{CR}} = L_{\text{em}}$ [2]. An exception are hypernovae. In addition, Ref. [63] argued that hypernovae can accelerate protons up to 10^{19} eV, if their ejecta have a rather flat energy distribution, $E_k \propto (\beta\Gamma)^{-2}$ (compared to $E_k \propto (\beta\Gamma)^{-5}$ for non-relativistic shocks).

4.4 Comments on the modelling of sources: Individual vs. average sources

Combined fits to the energy spectrum and the composition of UHECRs use often identical sources with a continuous spatial distribution. In this idealisation, one replaces sources which typically differ even within a specific source class in properties like their CR luminosity, maximal energy, and initial composition by an ‘‘average source’’ plus a redshift evolution of the emissivity. As an example how this idealisation affects the interpretation of such fits, one can consider the effect of a distribution of maximal energies [64]: Assuming for concreteness a power-law distribution for the maximal energies of the individual sources, $dn/dE_{\text{max}} \propto E_{\text{max}}^{-\beta}$, and a power law for the energy spectrum of individual sources, $dN_i/dE \propto E^{-\alpha}$, then the total energy spectrum of all sources

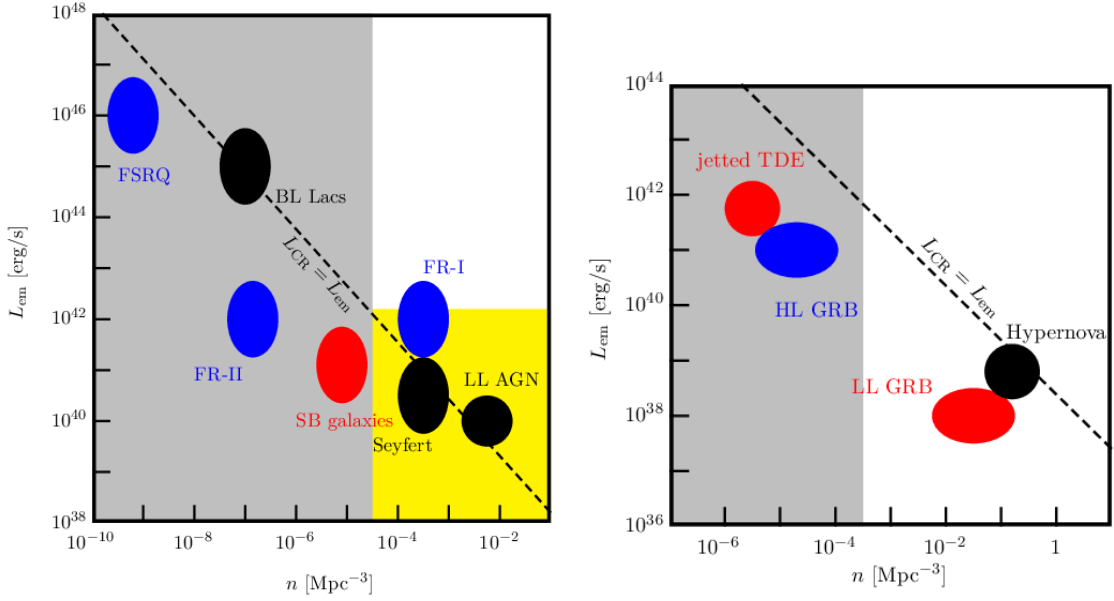


Figure 8: Combined constraints in the luminosity vs. number density plot shown for stationary (left) and transient (right) sources. The light-gray area is excluded by the absence of multiplets, the yellow area by the minimal luminosity argument.

becomes $dN_{\text{tot}}/dE \propto E^{1-\alpha-\beta}$ in the limit of $E_{\text{max}} \rightarrow \infty$, if they are otherwise identical. Thus the inferred slope agrees with the one of individual sources only for the special case $\beta = 1$.

A distribution of luminosities and maximal energies will reduce the number of active sources at the highest energies. For a smaller number of sources, the likelihood to find small breaks in the spectrum will increase. In this picture, it is natural that new features like the “instep” show up in the energy spectrum as experimental errors are reduced.

5. Specific models

5.1 Active galactic nuclei

Radio galaxies Fanaroff-Riley radio galaxies are long-standing candidates for UHECR sources. In addition to the well-established types of FR-I and FR-II galaxies, FR-0 galaxies as their low-luminosity extension were suggested in Ref. [65] as accelerator of UHECRs. These authors argued that FR-0 galaxies have the required emissivity to power the observed UHECR energy density, while their rather high density would lead to an almost isotropic contribution to the UHECR flux. Their average jet luminosity of $10^{42} - 10^{43}$ erg/s is above the Blandford limit. However, acceleration up to the highest observed energies is possible only if hybrid acceleration, i.e. a combination of first-order Fermi with gradual shear acceleration, is realized in these sources.

Blazars Gamma-ray blazars have attracted special attention, since IceCube detected several events from the direction of TXS 0506+056 and PKS 1502+106; see the highlight talk of Foteini Oikonomou for an extensive discussion [66]. An example for these works is Ref. [67], which modelled the populations of low- and high-luminosity blazars together with FSRQs. The

measured spectrum and composition of UHECRs is roughly reproduced in this model above 10^{18} eV. At the same time, the resulting neutrino fluxes produced inside the AGN jets can obey the IceCube stacking limits in the PeV range, while still giving a significant flux of EeV neutrinos.

NGC 1068 The Seyfert II galaxy NGC 1068 has attracted also special attention, because of a possible excess of IceCube events [68]. At the same time, MAGIC [69] reported an upper limit to the gamma-ray flux above 200 GeV, requiring that the gamma-rays accompanying the neutrino flux must be strongly attenuated in the source. The authors of Ref. [70] gave an updated flux prediction for this AGN using the Stecker-Donner-Salamon-Sommers AGN core model and argued that it can accommodate the IceCube excess. The authors of Ref. [71] considered instead the inner regions of the wind launched by the accretion disk. They found that pp interactions with gas may explain the observations, if the gas densities are in the range typical for clouds in the broadline region. NGC 1068 is not only an AGN, but also a starburst galaxy. The authors of Ref. [72] stressed the need to model both the AGN core and the circumnuclear starburst region in order to provide a complete description of the non-thermal phenomena of AGN-starburst composite galaxies.

5.2 Starburst galaxies

The evidence for a correlation of UHECR arrival directions with the positions of nearby starburst galaxies poses the question if plausible model for UHECR acceleration in these galaxies can be developed. A natural acceleration site is the termination shock of the strong galactic wind expected in starburst galaxies. The maximal energy achievable for protons,

$$E_{\max} \simeq 10^{17} \text{eV} (t_{\text{acc}}/10^9 \text{yr})(B/0.3 \mu\text{G})(v_{\text{sh}}/1000 \text{km/s}),$$

depends on the lifetime of the galactic outflows. Typically, they persist only for times much smaller than the age of galaxies, $t_{\text{acc}} \sim (10 - 100) \text{Myr}$ [73], and thus E_{\max} is too small. The Blandford condition supports this conclusion. In the model of Ref. [74], acceleration of protons to EeV energies require winds with extreme injection power, $L \sim (10^{44} - 10^{45}) \text{erg/s}$, beyond what is observed in starburst galaxies. Consequently, most works on starburst galaxies at this ICRC concentrated on the acceleration of CRs up to energies to tens of PeV, and the associated production of neutrinos, see e.g. Refs. [75, 76].

In an alternative view, a starburst galaxy may not be a UHECR accelerator as an entity but due to its high rate of GRBs, hypernovae, or pulsars. An open question is then if starburst galaxies act as a superposition of single sources, or if the specific environment and collective effects are important. In the former case, we recall that the maximal energy achievable in small sources like pulsars is typically reduced relative to the naive expectation, while the emissivity of GRBs is too low. Only hypernovae may satisfy both constraints, and explain in addition the observed correlations with UHECR arrival directions.

5.3 Gamma-ray bursts

Gamma-ray bursts became primary candidates as UHECR and high-energy neutrino sources, after the so-called Γ^2 acceleration mechanisms⁴ was suggested [60, 78]. However, the large escape

⁴A modern incarnation is the espresso mechanism discussed in Ref. [77] for AGN jets.

probability from relativistic shocks after the first cycle restrict the energy gain per cycle to a factor of order unity, making them much less effective accelerators as initially suggested [79, 80]. Moreover, their emissivity $Q \sim 10^{43} \text{ erg/Mpc}^3 \text{ yr}$ is at least a factor ten too low to explain the observed UHECR flux above the ankle. Finally, the prediction that GRBs are also sources of high-energy neutrinos allowed the search of correlations with IceCube events. From the absence of correlations in the neutrino data, lower bounds on the number density of the sources can be derived, excluding effective densities below $10^{-6}/\text{Mpc}^3$ [81]. These constraints from IceCube apply to high-luminosity GRBs and require either a very low E_{max} or a small baryon load. Either way, this excludes high-luminosity GRBs as major UHECR sources.

As a remedy, it was suggested that low-luminosity GRBs, i.e. GRBs with $L \sim (10^{46} - 10^{49}) \text{ erg/s}$, may be able to power the UHECR flux. In addition to the general problem of the too small GRB emissivity, it is unclear if high enough energies are achievable in these sources which probably contain shocks in the transrelativistic regime. For the special case of GRB 060218, it was argued that effective acceleration is excluded both in the prompt and afterglow phase [82]. On the other hand, the authors of Ref. [83] argued for GRB 980425 that heavy nuclei can reach energies up to 10^{20} eV , if the source is rather extended. This variation between different low-luminosity GRBs may indicate that they do not form a single physical source class.

6. Conclusions

The field of UHECRs has seen considerable experimental progress in the last decade. The energy spectrum is measured precisely and has revealed a new feature, the instep. The first clear detection of an anisotropy in the UHECR intensity is a dipole with a 6% amplitude at energies $\geq 8 \times 10^{18} \text{ eV}$ and a direction which points towards the Galactic anticentre. Thus UHECR experiments resolve for the first time the non-uniformity in the local distribution of UHECR sources. Additionally, the PAO claims evidence for a correlation of the UHECR arrival directions with specific types of UHECR sources, most significant with starburst galaxies. However, the smearing angle used in this study is large, and some confusion between different source classes (e.g. due to AGN-starburst composites) may occur.

Combining experimental and theoretical constraints on the number density and luminosity of UHECR sources, luminous and numerous AGN types as FR-I and Seyfert galaxies, or alternatively hypernovae, appear as the most promising UHECR sources. In the latter case, the increased hypernovae rate in starburst galaxies may explain the suggested correlation of their positions with UHECR arrival directions.

The determination of the mass composition of UHECRs has progressed too. The PAO composition data suggest the presence of a Peters cycle above $2 \times 10^{18} \text{ eV}$, with well separated elemental groups at different energies. Since this scenario requires in the simplest models very hard injection spectra, it should be scrutinised further. In particular, after its extension and upgrade, TA should be able to confirm or to challenge these results. Moreover, the upgrades of TA and the PAO are important steps towards the future identification of a proton (or light) component on an event-by-event basis which is required to improve correlation analyses with specific source classes.

On the theoretical side, it is desirable to abandon the idea of average sources and to develop and to employ instead models which include physically motivated parameters for individual

sources. Exploring in detail the multi-messenger connections will be another important step towards understanding the sources of UHECRs. Hypernova explosions and particle acceleration in their trans-relativistic shocks deserve more thorough studies.

Acknowledgments

It is a pleasure to thank all my collaborators, and in particular Dima Semikoz, for fruitful discussions and work on topics related to this review. I would like to thank also Björn Eichmann and Michael Unger for comments on this article.

References

- [1] Y. Tsunesada, R. Abbasi, T. Abu-Zayyad, M. Allen, Y. Arai, R. Arimura et al., *Joint analysis of the energy spectrum of ultra-high-energy cosmic rays as measured at the Pierre Auger Observatory and the Telescope Array*, *PoS ICRC2021* (2021) 337.
- [2] V. Berezhinsky, A. Z. Gazizov and S. I. Grigorieva, *On astrophysical solution to ultrahigh-energy cosmic rays*, *Phys. Rev.* **D74** (2006) 043005 [[hep-ph/0204357](#)].
- [3] PIERRE AUGER collaboration, A. Aab et al., *Features of the Energy Spectrum of Cosmic Rays above 2.5×10^{18} eV Using the Pierre Auger Observatory*, *Phys. Rev. Lett.* **125** (2020) 121106 [[2008.06488](#)].
- [4] PIERRE AUGER collaboration, A. Aab et al., *Measurement of the cosmic-ray energy spectrum above 2.5×10^{18} eV using the Pierre Auger Observatory*, *Phys. Rev. D* **102** (2020) 062005 [[2008.06486](#)].
- [5] PIERRE AUGER collaboration, A. Castellina, *Highlights from the Pierre Auger Observatory*, *PoS ICRC2019* (2021) 004 [[1909.10791](#)].
- [6] PIERRE AUGER collaboration, A. Aab et al., *Inferences on mass composition and tests of hadronic interactions from 0.3 to 100 EeV using the water-Cherenkov detectors of the Pierre Auger Observatory*, *Phys. Rev.* **D96** (2017) 122003 [[1710.07249](#)].
- [7] PIERRE AUGER collaboration, J. Bellido, *Depth of maximum of air-shower profiles at the Pierre Auger Observatory: Measurements above $10^{17.2}$ eV and Composition Implications*, *PoS ICRC2017* (2018) 506.
- [8] TELESCOPE ARRAY collaboration, R. U. Abbasi et al., *Depth of Ultra High Energy Cosmic Ray Induced Air Shower Maxima Measured by the Telescope Array Black Rock and Long Ridge FADC Fluorescence Detectors and Surface Array in Hybrid Mode*, *Astrophys. J.* **858** (2018) 76 [[1801.09784](#)].
- [9] T. Bergmann, R. Engel, D. Heck, N. N. Kalmykov, S. Ostapchenko, T. Pierog et al., *One-dimensional Hybrid Approach to Extensive Air Shower Simulation*, *Astropart. Phys.* **26** (2007) 420 [[astro-ph/0606564](#)].
- [10] R. Alves Batista et al., *Open Questions in Cosmic-Ray Research at Ultrahigh Energies*, *Front. Astron. Space Sci.* **6** (2019) 23 [[1903.06714](#)].
- [11] PIERRE AUGER, TELESCOPE ARRAY collaboration, A. Yushkov, “Report of the Auger-TA Working Group on the Composition of UHECRs.”
- [12] M. Unger, G. R. Farrar and L. A. Anchordoqui, *Origin of the ankle in the ultrahigh energy cosmic ray spectrum, and of the extragalactic protons below it*, *Phys. Rev.* **D92** (2015) 123001 [[1505.02153](#)].
- [13] M. Kachelrieß, O. Kalashev, S. Ostapchenko and D. V. Semikoz, *Minimal model for extragalactic cosmic rays and neutrinos*, *Phys. Rev.* **D96** (2017) 083006 [[1704.06893](#)].
- [14] E. Guido, P. Abreu, M. Aglietta, J. M. Albury, I. Allekotte, A. Almela et al., *Combined fit of the energy spectrum and mass composition across the ankle with the data measured at the Pierre Auger Observatory*, *PoS ICRC2021* (2021) 311.
- [15] PIERRE AUGER collaboration, M. Unger, *Highlights from the Pierre Auger Observatory*, *PoS ICRC2017* (2018) 1102 [[1710.09478](#)].
- [16] M. Kachelrieß, *Anisotropies and clustering of extragalactic cosmic rays*, *Nucl. Phys. B Proc. Suppl.* **165** (2007) 272 [[astro-ph/0610862](#)].
- [17] M. Kachelrieß and P. D. Serpico, *The Compton-Getting effect on ultra-high energy cosmic rays of cosmological origin*, *Phys. Lett.* **B640** (2006) 225 [[astro-ph/0605462](#)].

- [18] M. Kachelrieß, P. D. Serpico and M. Teshima, *The Galactic magnetic field as spectrograph for ultrahigh energy cosmic rays*, *Astropart. Phys.* **26** (2006) 378 [astro-ph/0510444].
- [19] A. Cuoco, R. D’Abrusco, G. Longo, G. Miele and P. D. Serpico, *The footprint of large scale cosmic structure on the ultrahigh energy cosmic ray distribution*, *JCAP* **01** (2006) 009 [astro-ph/0510765].
- [20] M. Kachelrieß and D. V. Semikoz, *Clustering of ultrahigh energy cosmic ray arrival directions on medium scales*, *Astropart. Phys.* **26** (2006) 10 [astro-ph/0512498].
- [21] PIERRE AUGER collaboration, A. Aab et al., *Observation of a Large-scale Anisotropy in the Arrival Directions of Cosmic Rays above 8×10^{18} eV*, *Science* **357** (2017) 1266 [1709.07321].
- [22] PIERRE AUGER collaboration, A. Aab et al., *Large-scale cosmic-ray anisotropies above 4 EeV measured by the Pierre Auger Observatory*, *Astrophys. J.* **868** (2018) 4 [1808.03579].
- [23] P. Erdogdu et al., *The Dipole anisotropy of the 2 Micron All-Sky Redshift Survey*, *Mon. Not. Roy. Astron. Soc.* **368** (2006) 1515 [astro-ph/0507166].
- [24] TELESCOPE ARRAY, PIERRE AUGER collaboration, P. Tinyakov et al., *The UHECR dipole and quadrupole in the latest data from the original Auger and TA surface detectors*, *PoS ICRC2021* (2021) 375 [2111.14593].
- [25] A. di Matteo, L. A. Anchordoqui, T. Bister, J. Biteau, L. Caccianiga, R. M. de Almeida et al., *UHECR arrival directions in the latest data from the original Auger and TA surface detectors and nearby galaxies*, *PoS ICRC2021* (2021) 308.
- [26] PIERRE AUGER collaboration, A. Aab et al., *An Indication of anisotropy in arrival directions of ultra-high-energy cosmic rays through comparison to the flux pattern of extragalactic gamma-ray sources*, *Astrophys. J.* **853** (2018) L29 [1801.06160].
- [27] TELESCOPE ARRAY, PIERRE AUGER collaboration, A. di Matteo et al., *UHECR arrival directions in the latest data from the original Auger and TA surface detectors and nearby galaxies*, *PoS ICRC2021* (2021) 308 [2111.12366].
- [28] V. Berezhinsky, A. Z. Gazizov and S. I. Grigorieva, *Dip in UHECR spectrum as signature of proton interaction with CMB*, *Phys. Lett.* **B612** (2005) 147 [astro-ph/0502550].
- [29] G. Giacinti, M. Kachelrieß, D. V. Semikoz and G. Sigl, *Cosmic Ray Anisotropy as Signature for the Transition from Galactic to Extragalactic Cosmic Rays*, *JCAP* **1207** (2012) 031 [1112.5599].
- [30] A. W. Strong, J. Wdowczyk and A. W. Wolfendale, *The gamma-ray background: a consequence of metagalactic cosmic ray origin?*, *Journal of Physics A Mathematical General* **7** (1974) 120.
- [31] V. S. Berezhinsky and A. Yu. Smirnov, *Cosmic neutrinos of ultra-high energies and detection possibility*, *Astrophys. Space Sci.* **32** (1975) 461.
- [32] FERMI-LAT collaboration, M. Ackermann et al., *The spectrum of isotropic diffuse gamma-ray emission between 100 MeV and 820 GeV*, *Astrophys. J.* **799** (2015) 86 [1410.3696].
- [33] O. E. Kalashev, D. V. Semikoz and G. Sigl, *Ultra-High Energy Cosmic Rays and the GeV-TeV Diffuse Gamma-Ray Flux*, *Phys. Rev.* **D79** (2009) 063005 [0704.2463].
- [34] V. Berezhinsky, A. Gazizov, M. Kachelrieß and S. Ostapchenko, *Restricting UHECRs and cosmogenic neutrinos with Fermi-LAT*, *Phys. Lett.* **B695** (2011) 13 [1003.1496].
- [35] J. Heinze, D. Boncioli, M. Bustamante and W. Winter, *Cosmogenic Neutrinos Challenge the Cosmic Ray Proton Dip Model*, *Astrophys. J.* **825** (2016) 122 [1512.05988].
- [36] M. Kachelrieß and D. V. Semikoz, *Cosmic Ray Models*, *Prog. Part. Nucl. Phys.* **109** (2019) 103710 [1904.08160].
- [37] FERMI-LAT collaboration, M. Ackermann et al., *Resolving the Extragalactic γ -Ray Background above 50 GeV with the Fermi Large Area Telescope*, *Phys. Rev. Lett.* **116** (2016) 151105 [1511.00693].
- [38] V. S. Berezhinsky, S. V. Bulanov, V. A. Dogiel and V. S. Ptuskin, *Astrophysics of cosmic rays*. Amsterdam, Netherlands: North-Holland, 1990.
- [39] M. Kachelrieß, S. Ostapchenko and R. Tomàs, *ELMAG: A Monte Carlo simulation of electromagnetic cascades on the extragalactic background light and in magnetic fields*, *Comput. Phys. Commun.* **183** (2012) 1036 [1106.5508].
- [40] W. D. Apel et al., *KASCADE-Grande measurements of energy spectra for elemental groups of cosmic rays*, *Astropart. Phys.* **47** (2013) 54 [1306.6283].
- [41] ICECUBE collaboration, M. G. Aartsen et al., *Observation and Characterization of a Cosmic Muon Neutrino Flux from the Northern Hemisphere using six years of IceCube data*, *Astrophys. J.* **833** (2016) 3 [1607.08006].

- [42] ICECUBE collaboration, M. G. Aartsen et al., *The IceCube Neutrino Observatory - Contributions to ICRC 2017 Part II: Properties of the Atmospheric and Astrophysical Neutrino Flux*, [1710.01191](#).
- [43] I. Tamborra, "Multi-Messenger." Rapporteur talk at the "37th International Cosmic Ray Conference", Berlin, 2021.
- [44] T. Jaffe, "Constraining Magnetic Fields at Galactic Scales ." Review talk at the "37th International Cosmic Ray Conference", Berlin.
- [45] G. Giacinti, M. Kachelrieß and D. V. Semikoz, *Reconciling cosmic ray diffusion with Galactic magnetic field models*, *JCAP* **1807** (2018) 051 [[1710.08205](#)].
- [46] M. S. Pshirkov, P. G. Tinyakov and F. R. Urban, *New limits on extragalactic magnetic fields from rotation measures*, *Phys. Rev. Lett.* **116** (2016) 191302 [[1504.06546](#)].
- [47] K. Jedamzik and A. Saveliev, *Stringent Limit on Primordial Magnetic Fields from the Cosmic Microwave Background Radiation*, *Phys. Rev. Lett.* **123** (2019) 021301 [[1804.06115](#)].
- [48] FERMI-LAT collaboration, M. Ackermann et al., *The Search for Spatial Extension in High-latitude Sources Detected by the Fermi Large Area Telescope*, *Astrophys. J. Suppl.* **237** (2018) 32 [[1804.08035](#)].
- [49] A. E. Broderick, P. Tiede, P. Chang, A. Lamberts, C. Pfrommer, E. Puchwein et al., *Missing Gamma-ray Halos and the Need for New Physics in the Gamma-ray Sky*, *Astrophys. J.* **868** (2018) 87 [[1808.02959](#)].
- [50] E. Waxman and J. Miralda-Escude, *Images of bursting sources of high-energy cosmic rays. I. Effects of magnetic fields*, *Astrophys. J.* **472** (1996) L89 [[astro-ph/9607059](#)].
- [51] J. Miralda-Escude and E. Waxman, *Signatures of the origin of high-energy cosmic rays in cosmological gamma-ray bursts*, *Astrophys. J.* **462** (1996) L59 [[astro-ph/9601012](#)].
- [52] E. Parizot, *GZK horizon and magnetic fields*, *Nucl. Phys. Proc. Suppl.* **136** (2004) 169 [[astro-ph/0409191](#)].
- [53] V. Berezhinsky and A. Z. Gazizov, *Diffusion of cosmic rays in expanding universe*, *Astrophys. J.* **643** (2006) 8 [[astro-ph/0512090](#)].
- [54] PIERRE AUGER collaboration, P. Abreu et al., *Bounds on the density of sources of ultra-high energy cosmic rays from the Pierre Auger Observatory*, *JCAP* **05** (2013) 009 [[1305.1576](#)].
- [55] A. T. Steffen, A. J. Barger, L. L. Cowie, R. F. Mushotzky and Y. Yang, *The changing AGN population*, *Astrophys. J. Lett.* **596** (2003) L23 [[astro-ph/0308238](#)].
- [56] M. Kachelrieß, *Lecture notes on high energy cosmic rays*, [0801.4376](#).
- [57] K. V. Ptitsyna and S. V. Troitsky, *Physical conditions in potential sources of ultra-high-energy cosmic rays. I. Updated Hillas plot and radiation-loss constraints*, *Phys. Usp.* **53** (2010) 691 [[0808.0367](#)].
- [58] R. V. E. Lovelace, *Dynamo model of double radio sources*, *Nature* **262** (1976) 649.
- [59] R. D. Blandford, *Acceleration of ultrahigh-energy cosmic rays*, *Phys. Scripta* **T85** (2000) 191 [[astro-ph/9906026](#)].
- [60] E. Waxman, *Cosmological gamma-ray bursts and the highest energy cosmic rays*, *Phys. Rev. Lett.* **75** (1995) 386 [[astro-ph/9505082](#)].
- [61] M. Lemoine and G. Pelletier, *On electromagnetic instabilities at ultra-relativistic shock waves*, *Mon. Not. Roy. Astron. Soc.* **402** (2010) 321 [[0904.2657](#)].
- [62] K. Murase and H. Takami, *Implications of Ultra-High-Energy Cosmic Rays for Transient Sources in the Auger Era*, *Astrophys. J. Lett.* **690** (2009) L14 [[0810.1813](#)].
- [63] X.-Y. Wang, S. Razzaque, P. Meszaros and Z.-G. Dai, *High-energy Cosmic Rays and Neutrinos from Semi-relativistic Hypernovae*, *Phys. Rev. D* **76** (2007) 083009 [[0705.0027](#)].
- [64] M. Kachelrieß and D. V. Semikoz, *Reconciling the ultra-high energy cosmic ray spectrum with Fermi shock acceleration*, *Phys. Lett. B* **634** (2006) 143 [[astro-ph/0510188](#)].
- [65] L. Merten, M. Boughelilba, A. Reimer, P. Da Vela, S. Vorobiov, F. Tavecchio et al., *FR-0 jetted active galaxies: extending the zoo of candidate sites for UHECR acceleration*, *PoS ICRC2021* (2021) 986 [[2107.13278](#)].
- [66] F. Oikonomou, *High-energy neutrino emission from blazars*, *PoS ICRC2021* (2021) 030.
- [67] X. Rodrigues et al., "Active galactic nuclei as neutrino sources in the PeV and EeV regimes." Contribution 1321 at the "37th International Cosmic Ray Conference", Berlin, 2021.
- [68] ICECUBE collaboration, M. G. Aartsen et al., *Time-Integrated Neutrino Source Searches with 10 Years of IceCube Data*, *Phys. Rev. Lett.* **124** (2020) 051103 [[1910.08488](#)].
- [69] MAGIC collaboration, V. A. Acciari et al., *Constraints on gamma-ray and neutrino emission from NGC 1068 with the MAGIC telescopes*, *Astrophys. J.* **883** (2019) 135 [[1906.10954](#)].

- [70] L. A. Anchordoqui, J. Krizmanic and F. Stecker, *High-Energy Neutrinos from NGC 1068*, *PoS ICRC2021* (2021) 993.
- [71] S. Inoue, M. Cerruti, K. Murase and R.-Y. Liu, *High-energy neutrinos and gamma rays from the AGN-driven wind in NGC 1068*, *PoS ICRC2021* (2021) 1013.
- [72] B. Eichmann, R.-J. Dettmar and J. Becker-Tjus, *An AGN-starburst composite multi-messenger model of NGC 1068*, *PoS ICRC2021* (2021) 1006.
- [73] G. E. Romero, A. L. Müller and M. Roth, *Particle acceleration in the superwinds of starburst galaxies*, *Astron. Astrophys.* **616** (2018) A57 [1801.06483].
- [74] E. Peretti, G. Morlino, P. Blasi, P. Cristofari and M. Ahlers, *Exploring galactic wind superbubbles by multimessenger observations*, *PoS ICRC2021* (2021) 995.
- [75] A. Condorelli, S. Petrer, D. Boncioli and E. Peretti, *Starburst Galaxies as possible sources of UHECRs and neutrinos*, *PoS ICRC2021* (2021) 959.
- [76] A. Marinelli, A. Ambrosone, M. Chianese, D. Fiorillo, G. Miele and O. Pisanti, *A novel multimessenger study of Starburst galaxies: implications for neutrino astronomy*, *PoS ICRC2021* (2021) 1232.
- [77] R. Mbarek, D. Caprioli and K. Murase, *Ultra-High-Energy Cosmic Rays and Neutrinos from relativistic jets of Active Galactic Nuclei*, *PoS ICRC2021* (2021) 481.
- [78] M. Vietri, *On the acceleration of ultrahigh-energy cosmic rays in gamma-ray bursts*, *Astrophys. J.* **453** (1995) 883 [astro-ph/9506081].
- [79] A. Achterberg, Y. A. Gallant, J. G. Kirk and A. W. Guthmann, *Particle acceleration by ultrarelativistic shocks: Theory and simulations*, *Mon. Not. Roy. Astron. Soc.* **328** (2001) 393 [astro-ph/0107530].
- [80] M. Lemoine, G. Pelletier and B. Revenu, *On the efficiency of Fermi acceleration at relativistic shocks*, *Astrophys. J. Lett.* **645** (2006) L129 [astro-ph/0606005].
- [81] M. Kowalski, *Status of High-Energy Neutrino Astronomy*, *J. Phys. Conf. Ser.* **632** (2015) 012039 [1411.4385].
- [82] F. Samuelsson, D. Begue, F. Ryde, A. Pe'er and K. Murase, *The problematic connection between low-luminosity gamma-ray bursts and ultra-high-energy cosmic rays*, *PoS ICRC2021* (2021) 467.
- [83] A. Rudolph, J. Heinze, D. Biehl, A. Fedynitch, D. Boncioli, Z. Bošnjak et al., *UHECR from high- and low-luminosity Gamma-Ray Bursts*, *PoS ICRC2021* (2021) 1000.